Visualization of human retinal and choroidal vascular networks with phase-variance optical coherence tomography

Dae Yu Kim,[1]* Jeff Fingler,[1] Robert J. Zawadzki[2], Malvika Verma,[1]
Daniel M. Schwartz,[3] John S. Werner,[2] and Scott E. Fraser[1]

[1]Biological Imaging Center, California Institute of Technology, Pasadena, CA,
[2]UC Davis Eye Center, University of California Davis, Sacramento, CA,
[3]Dept. of Ophthalmology, University of California San Francisco, San Francisco, CA;

ABSTRACT

We present *in vivo* noninvasive retinal and choroidal perfusion maps with phase-variance optical coherence tomography (pvOCT). We acquired a pvOCT volumetric data set of a normal subject and visualized blood circulation in the retina and the choroid. *En face* projection views of the retina as well as the choroid were generated from a manually segmented volumetric data set. In addition, the processed pvOCT images were compared to current standard imaging modalities used for retinal and choroidal vasculature visualization in clinical settings, including fluorescein angiography (FA) and indocyanine green angiography (ICGA).

Keywords: Optical coherence tomography; Phase contrast technique; Imaging system; Medical optics instrumentation

* dyukim@caltech.edu; phone 1 626 395-4499; fax 1 626 449-5163;

INTRODUCTION

The two major blood supplies in the posterior segment of the human eye are the retinal and choroidal circulation. Currently, fundus fluorescein angiography (FA) and indocyanine green angiography (ICGA) are the most widely used techniques to visualize the retinal vasculature and choroidal circulation in a clinical setting, respectively. Several noninvasive imaging methods have been developed to produce perfusion maps of both the retina and the choroid similar to FA and ICGA. These include dual-beam optical coherence angiography [1], optical micro-angiography [2], ultrahigh-speed widefield angiography [3], joint spectral and time-domain optical coherence tomography [4], phase-resolved optical frequency domain imaging [5], Doppler optical coherence angiography [6], and phase-variance OCT [7,8,9], each with different visualization capabilities and limitations. Two-dimensional circulation maps from the retinal layers acquired using the OCT based methods demonstrated analogous results to fundus FA. Unlike retinal vasculature, vessels in the choroid are located underneath the retinal pigment epithelium (RPE), a high scattering medium for light sources used in fundus FA and clinical OCT. Moreover, there are highly dense vascular supplies in the choroid over the macular region. Due to these reasons, fundus FA or OCT reflectance imaging does not provide all details of choroidal vascular circulation in the macular area.

In this manuscript, we demonstrate vessel networks in both retinal and choroidal layers extracted with phase-variance OCT (pvOCT). We imaged a healthy volunteer's retina over the parafoveal area and segmented between the retina and the choroid layer in RPE. In addition, we generated two-dimensional (2D) projection views of two vascular plexuses for comparison with fundus FA and ICGA images.

METHODS

Retinal images of a healthy 60-year-old male volunteer were acquired by a custom-built Fourier-domain OCT (Fd-OCT) system operating at 125,000 axial scans (A-scan) per second. Details of the system have been previously reported [9]. A 2.2 x 2.2mm^2 retinal area was acquired through a series of BM-scans, which are cross-sectional OCT images (B-scans)

Ophthalmic Technologies XXIII, edited by Fabrice Manns, Per G. Söderberg, Arthur Ho, Proc. of SPIE
Vol. 8567, 856702 · © 2013 SPIE · CCC code: 1605-7422/13/$18 · doi: 10.1117/12.2004606

acquired repeatedly over the same scan line. Phase changes were calculated through subtraction between consecutive B-scans acquired within each BM-scan. Motion contrast based phase-variance processing produced three-dimensional microcirculation images within the human retina. [7] *En face* projections of the two pvOCT volume data sets were used to create 2D vasculature maps. Finally, magnified fundus FA and ICGA images over the same retinal area were compared with the processed 2D perfusion maps created from pvOCT. The fundus angiographic images were acquired from the Heidelberg Spectralis (HRA+OCT).

RESULTS

Figure 1 (a) shows an averaged OCT reflectance (left) and a phase-variance processed image (right) from a single BM-scan, respectively, acquired over a lateral size of 2.2mm at a retinal position of approximately 6° temporal and 12° inferior to the fovea. In order to achieve better visualization of retinal circulation, we put the anterior surface of the subject's retina close to the zero path length difference position (a red dashed line in the Figure 1 (a)) where OCT imaging has maximum system sensitivity [10,11]. Here, red left and right braces demonstrate depth locations (approximately from the nerve fiber layer to the outer nuclear layer) of manual segmentation to generate maximum projection views. *An en face* projection of OCT intensity images from the volumetric data (2.2 x 2.2mm^2) is presented in Figure 1 (b). The maximum projection of the phase-variance processed data in the retinal layers over the same depths is shown in Figure 1 (c). Notice that the pvOCT image demonstrates enhanced contrast of microcapillaries compared to the OCT intensity projection view. A magnified FA image for the scanned area is shown in Figure 1 (d) to compare with the two projection views. Note that the quality of images in Figure 1 (c) and (d) is worse compared to perfusion maps previously demonstrated in the foveal region [7] because the optics in the OCT system have not been optimized to image the parafoveal retina (further away from the fovea).

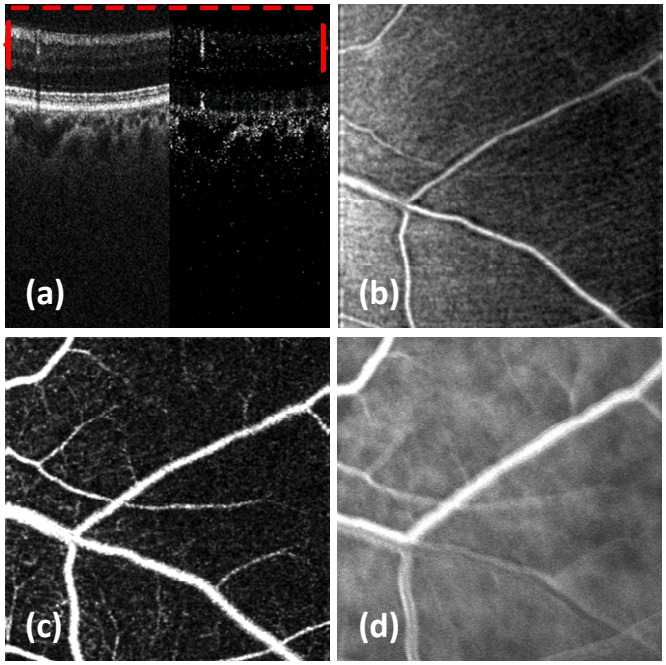

Figure 1. Visualization of retinal circulation with pvOCT of the healthy volunteer's left eye. 2.2 x 2.2 mm^2 volumetric scanning at a location 6° temporal and 12° inferior to the fovea of the retina. (a) An averaged OCT intensity image (left) and a phase-variance processed image (right) from one BM-scan (three B-scans). The zero path length difference position (red dashed line) is located above the anterior surface. Red braces indicate locations of manual segmentation. (b) A projection view of OCT intensity images from the volumetric data. (c) A projection view of phase-variance processed images from the volumetric OCT data. (d) A magnified FA image over the scanning area.

For enhancement of the OCT signal within the choroidal structure, we acquired 2.2 x 2.2 mm^2 volumetric data over the same scanning area as that of Figure 1 where the subject's choroid was aligned close to the zero path length difference position (a red dashed line in the Figure 2 (a)). Figure 2 (a) left and right images show an averaged OCT reflectance and a phase-variance processed imaging from a single BM-scan, respectively. In order to visualize choroidal feeder vessels, we segmented approximately 60μm depths (marked in red braces) starting at approximately 40μm below the retinal pigment epithelium layer from the volumetric data. Minimum projection of OCT intensity images from the segmented data is shown in Figure 2 (b). In addition, Figure 2 (c) demonstrates a projection view of the phase-variance OCT in the choroid. Notice that there is no intensity signal or phase-variance signal inside choroidal feeder vessels in Figure 2 (b) and (c). In this condition, we used minimum projection to obtain contrast images for choroidal vasculature. A cropped ICGA image for the scanned area is shown in Figure 2 (d) which contains retinal and choroidal vasculature networks.

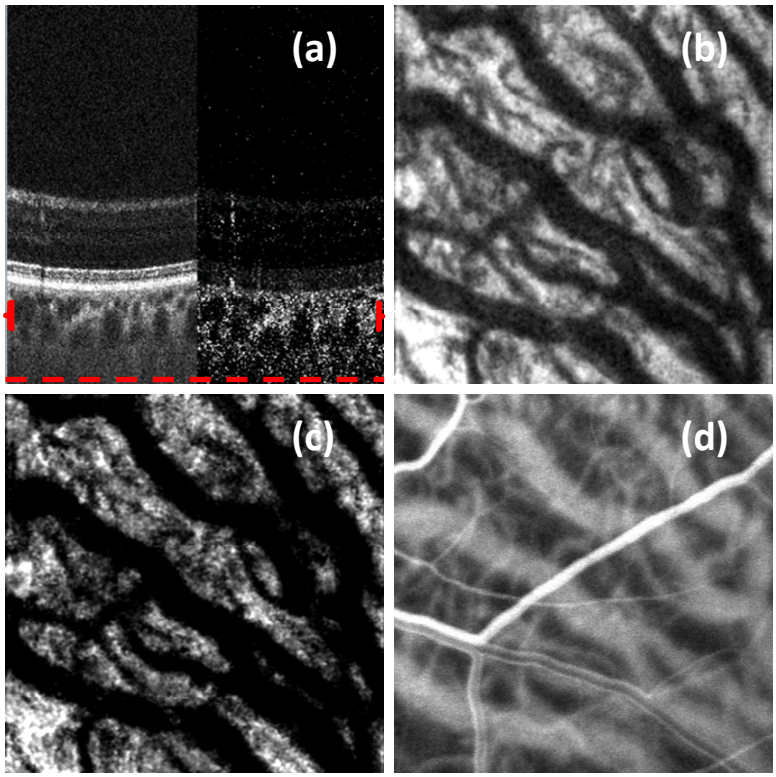

Figure 2. Visualization of choroidal feeder vessels with pvOCT of the healthy volunteer's left eye. 2.2 x 2.2 mm^2 volumetric scanning at a retinal position 6° temporal and 12° inferior to the fovea. (a) An averaged OCT intensity image (left) and a phase-variance processed image (right) from one BM-scan (three B-scans). The zero path length difference position (red dashed line) is located below the choroid. Red braces indicate locations of manual segmentation. (b) A minimum projection view of OCT intensity images from the volumetric data. (c) A minimum projection view of phase-variance processed images from the volumetric OCT data. (d) A magnified ICGA image over the scanning area.

In order to validate phase-variance processing in the larger diameter of choroidal vessels, we calculated the phase-variance contrast with different OCT intensity threshold levels within Figure 3. Figure 3 (b) shows a cross-sectional image (B-scan) of pvOCT with an intensity threshold at the background intensity level determined by Figure 3 (a). Figures 3 (c) and (d) demonstrate pvOCT B-scans with OCT intensity thresholding at 3dB and 6dB higher than the

same background intensity level, respectively. *En face* minimum projection images of the volumetric data, Figure 3 (a) ~ (d), segmented same depths used in Figure 2 within the choroid generates Figure 3 (e) - OCT intensity, (f) - pvOCT without thresholding, (g) - pvOCT with thresholding 3dB higher than the background intensity level, and (h) - pvOCT with thresholding 6dB higher than the background intensity level, respectively. Compared to projection views with different OCT intensity thresholding, we can notice that phase-variance values do not exist in feeder choroidal vessels. This may be caused by fringe washout of the spectrometer based Fd-OCT system for high flow rates in the vessels [12]. A table in the previous literature [13] summarized flow speeds of vasculature in the posterior eye obtained from human and animal studies where the flow velocity of the supply of choroidal vessels is approximately 50~100 times higher than that of microcapillaries in the retina.

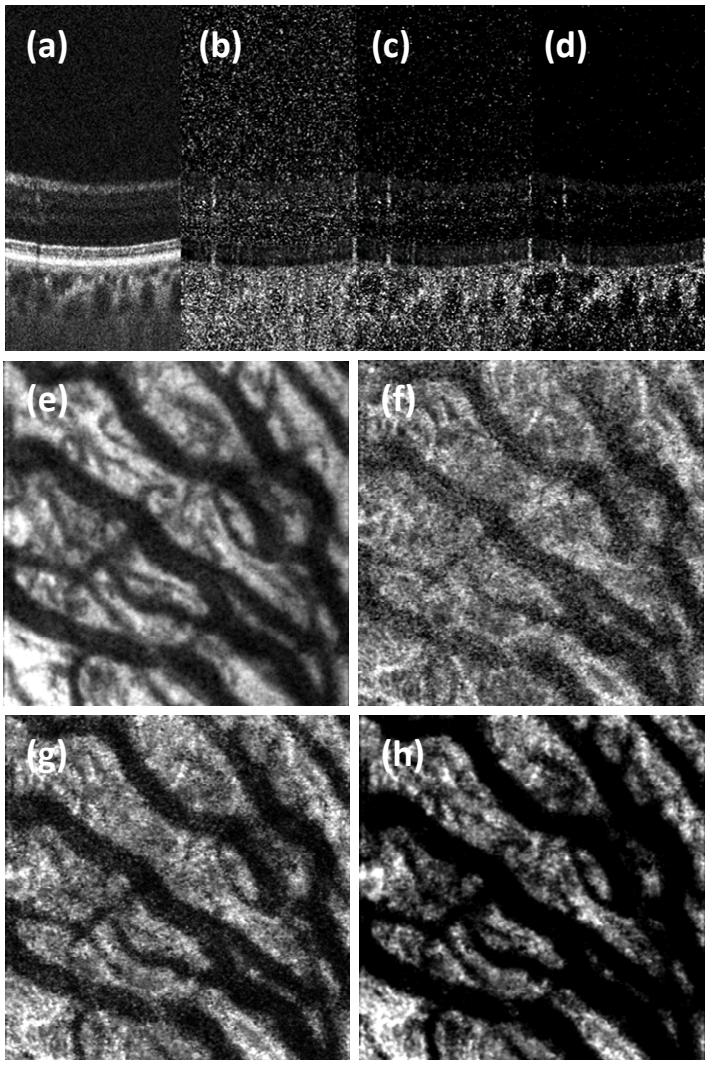

Figure 3. *En face* minimum projection views (2.2 x 2.2mm^2) of the volumetric data according to different OCT intensity thresholding values. (a) An averaged OCT intensity image from one BM-scan. (b) Phase-variance OCT processing with intensity thresholding at the background intensity level. (c) Phase-variance OCT processing with OCT intensity thresholding at 3dB higher than a background intensity level. (d) Phase-variance OCT processing with OCT intensity thresholding at 6dB higher than the background intensity level. (e) A projection view of OCT intensity imaging shown in (a) from the volumetric data. (f) A projection view of pvOCT imaging demonstrated in (b) from the volumetric data. (g) A projection view of pvOCT imaging shown in (c) from the volumetric data. (h) A projection view of pvOCT imaging shown in (b) from the volumetric data.

To combine retinal and choroidal perfusion maps using pvOCT, we made an inverse image of the projection view of the choroid in Figure 3 (h) and produced Figure 4 (b). The composite image of Figure 4 (c) shows vascular networks in the retina from Figure 4 (a), the maximum projection view from the volumetric pvOCT data segmented in the retina, as well as larger choroidal vessels from Figure 4 (b), inversing the minimum projection view from the volumetric pvOCT data segmented in the choroid. The combined perfusion map of Figure 4 (c) is comparable to the cropped ICGA image, Figure 4 (d), over the scanned region.

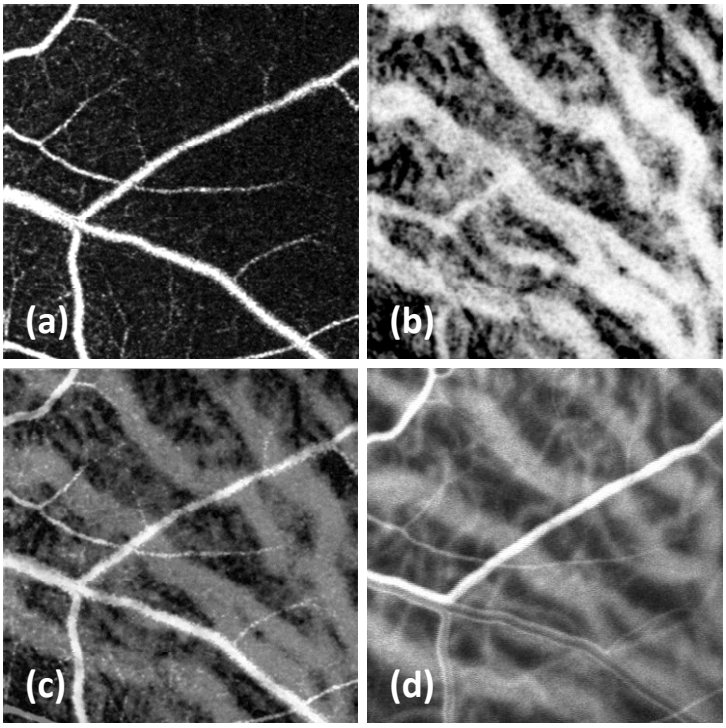

Figure 4. Visualizing retinal and choroidal perfusion maps (2.2 x 2.2mm^2). (a) A maximum projection view of the volumetric pvOCT data segmented in the retina. (b) Inversing the minimum projection view of the volumetric pvOCT data segmented in the choroid shown in Figure 3 (h). (c) A combined image of (a) and (b). (d) The zoomed-in ICGA image.

CONCLUSIONS

Phase-variance OCT allowed visualization of two-dimensional retinal and choroidal vessel networks comparable to fundus FA and ICGA. The *en face* view of choroidal circulation was created using minimum projection of the segmented volume, because there is no intensity or phase-variance OCT signal inside larger vessels, while phase-variance signals are present in the areas surrounding the larger vessels. Thus, pvOCT can be advantageous for non-invasive and more sensitive diagnosis of retinal and choroidal vascular diseases.

ACKNOWLEDGMENTS

This research was partially supported by Beckman Institute, That Man May See Foundation, National Eye Institute (EY 014743), and Research to Prevent Blindness (RPB).

REFERENCES

1. F. Jaillon, S. Makita, and Y. Yasuno, “Variable velocity range imaging of the choroid with dual-beam optical coherence angiography,” Opt. Express 20(1), 385–396 (2012)
2. R. Wang, L. An, P. Francis, and D. Wilson, “Depth-resolved imaging of capillary networks in retina and choroid using ultrahigh sensitive optical microangiography,” Opt. Lett. 35(9), 1467–1469 (2010).
3. C. Blatter, T. Klein, B.Grajciar, T. Schmoll, W. Wieser, R. Andre, R. Huber, and R. Leitgeb, "Ultrahigh-speed non-invasive widefield angiography", J. Biomed. Opt. 17, 070505 (2012)
4. A. Szkulmowska, M. Szkulmowski, D. Szlag, A. Kowalczyk, and M. Wojtkowski, "Three-dimensional quantitative imaging of retinal and choroidal blood flow velocity using joint Spectral and Time domain Optical Coherence Tomography," Opt. Express 17, 10584-10598 (2009)
5. B. Braaf, K. Vermeer, V. Sicam, E. van Zeeburg, J. van Meurs, and J. de Boer, "Phase-stabilized optical frequency domain imaging at 1-μm for the measurement of blood flow in the human choroid," Opt. Express 19, 20886-20903 (2011)
6. Y. Hong, S. Makita, F. Jaillon, M. Ju, E. Min, B. Lee, M. Itoh, M. Miura, and Y. Yasuno, "High-penetration swept source Doppler optical coherence angiography by fully numerical phase stabilization," Opt. Express 20, 2740-2760 (2012)
7. D. Kim, J. Fingler, J. Werner, D. Schwartz, S. Fraser, and R. Zawadzki, "In vivo volumetric imaging of human retinal circulation with phase-variance optical coherence tomography," Biomed. Opt. Express 2, 1504-1513 (2011)
8. D. Kim, J. Fingler, R. Zawadzki, S. Park, L. Morse, D. Schwartz, S. Fraser, and J. Werner, “Noninvasive imaging of the foveal avascular zone with high-speed, phase-variance optical coherence tomography,” Invest. Ophthalmol. Vis. Sci. 53, 85-92 (2012)
9. J. Fingler, R. Zawadzki, J. Werner, D. Schwartz, and S. Fraser, "Volumetric microvascular imaging of human retina using optical coherence tomography with a novel motion contrast technique," Opt. Express 17, 22190-22200 (2009)
10. D. Kim, J. Werner, and R. Zawadzki, " Comparison of phase-shifting techniques for in vivo full-range, high-speed Fourier-domain optical coherence tomography," J. Biomed. Opt. 15, 056011 (2010)
11. D. Kim, J. Werner, and R. Zawadzki, "Complex conjugate artifact-free adaptive optics optical coherence tomography of in vivo human optic nerve head," J. Biomed. Opt. 17, 126005 (2012)
12. H. Hendargo, R. McNabb, A. Dhalla, N. Shepherd, and J. Izatt, “Doppler velocity detection limitations in spectrometer-based versus swept-source optical coherence tomography,” Biomed. Opt. Express 2, 2175-2188 (2011)
13. B. Braaf, K. Vermeer, K. Vienola, and J. de Boer, “Angiography of the retina and the choroid with phase-resolved OCT using interval-optimized backstitched B-scans,” Opt. Express 20, 20516-20534 (2012).